North-Holland, Amsterdam

SPEG: AN ENERGY LOSS SPECTROMETER FOR GANIL

L. BIANCHI, B. FERNANDEZ, J. GASTEBOIS and A. GILLIBERT

Service de Physique Nucléaire Basse Energie, CEN Saclay, 91191 Gif-sur-Yvette, France

W. MITTIG

GANIL, B.P. 5027, 14021 Caen Cedex, France

J. BARRETTE

Foster Radiation Laboratory, Mc Gill University, Montréal, PQ, Canada

Received 9 September 1988

Since July 1985, an energy loss spectrometer (SPEG) is under operation at the National Heavy Ion Laboratory (GANIL), at Caen (France). It has been designed to allow the study of quantum states populated in reactions induced by nuclei accelerated at energies up to 100A MeV.

The spectrometer has been designed by P. Birien. The optical properties and the main magnetic features have been calculated by Birien and Valero. A detailed reported of their study is given in ref. [1].

In the first part of the present paper, after recalling the specifications of the spectrometer, we shall give an overall description of the main characteristics, together with indications about the various shimming procedures which have been used to achieve the desired resolution (sections 1–4).

In the second part, we shall describe various accessories and the different kinds of detectors which are used during experiments, with several illustrations of experimental results (sections 5 and 6).

1. Main specifications

The following main requirements were taken into account in designing the spectrometer:

(1) The momentum resolution (dp/p) must be around 10^{-4}, which leads to a few hundred keV in energy resolution for incident light ions at maximum energy (^{12}C, ^{16}O, ^{20}Ne at 100A MeV). This implies an energy loss spectrometer to be built, because the beam momentum resolution is not better than 5×10^{-4}. It also implies a focal dispersion high enough so that the resolutions of the detectors allow the needed momentum resolution. A value of 8 m has been chosen ($dp/p = 10^{-4}$ then corresponds to 0.8 mm in position).

(2) In order to be able to perform coincidence experiments with good efficiency, a large solid angle as well as a wide range of analysed momenta was required. The actual values are respectively ~ 5 msr and 7% (i.e. a focal length ~ 60 cm, and an energy range higher than 150 MeV for 100A MeV ions).

(3) Due to the very strong forward peaking of the angular distributions at high energies, the spectrometer should allow zero degree and small angle measurements: as a solution, a C-shape has been chosen for all magnetic elements of the spectrometer, except for the last quadrupole lens. This makes it easy to set beam catchers anywhere inside, according to experimental requirements.

(4) As heavy ion induced reactions present large kinematic effects, the ejectile energy spreading induced by incident beam angular divergence would be prohibitive if the horizontal focus of the beam line would be kept on the target. It was therefore necessary to provide an easy way to move it as a function of the kinematic conditions (see refs. [2] and [3]). Furthermore, the displacement of the spectrometer focal plane has to be controlled. The last quadrupole lens Q2 (see fig. 1) has been designed for that purpose. This opens two main possibilities: either to keep the focal plane at a fixed position and thus to have dispersion values according to kinematic conditions, or to have a fixed dispersion value, but variable focal plane positions. In the latter case, the last quadrupole lens has to be adjusted to achieve a zero value for the angular dispersion. From the experience gained using the spectrometer, it is the most frequently used mode.

0168-9002/89/$03.50

2. General optical properties

SPEG consists of an analysing beam line coupled to a spectrometer, the whole set being achromatic.

Fig. 1 represents an overview of the spectrometer, where the different elements discussed below are identified.

2.1. The analysis beam line (see figs. 1–3)

The main characteristics are given in table 1, together with the first order matrix elements which describe the beam line from the object slits down to the target, for the nominal case (no kinematics).

The optics of GANIL is such that the beam transport system is achromatic down to the object slits. Then the beam profile is such as shown in fig. 3, for nominal values of the momentum spread ($dp/p = \pm 5 \times 10^{-3}$) and emittance ($5\pi$ mm mrad, leading to an angular divergence of ± 2.5 mrad in both planes). The first two lenses (QA1 and QA provide an intermediate focusing in front of the dipole (DA): real horizontal focusing and virtual vertical focusing (see fig. 3).

The two last lenses (QA3 and QA4) achieve the dispersion matching with the spectrometer.

Second order corrections are provided via mechanical and electrical shims installed inside the dipole, and via the two sextupole lenses (SA1 and SA2).

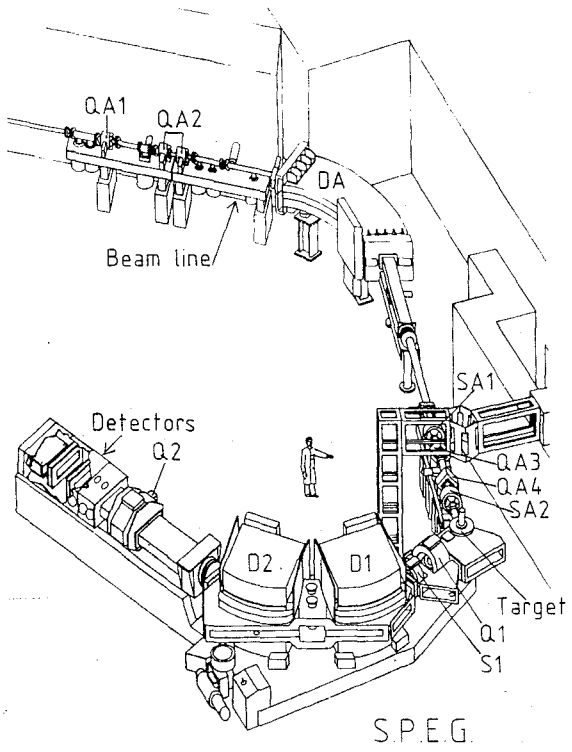

Fig. 1. Aristic view of SPEG.

Table 1
(1) Nominal characteristics of the dispersive beam line [a]

Dispersion on target	[m]	9.86
Horizontal magnification		0.175
Vertical magnification		1.0
Mean bending radius	[m]	3
Mean deflection angle	[deg]	75
Dipole entrance face angle	[deg]	23.5
Pole gap of the dipole	[mm]	150
Maximum dipole induction	[T]	1
Power required for maximum field	[kW]	140
Weight of the dipole	[t]	30

(2) Transport matrix elements of the beam line [b]

0.17593	0.00000	0.00000	0.00000	0.00000	9.86000
9.00131	5.68418	0.00000	0.00000	0.00000	−33.24957
0.00000	0.00000	−1.07312	0.00000	0.00000	0.00000
0.00000	0.00000	9.60682	−0.93185	0.00000	0.00000
9.64024	5.60461	0.00000	0.00000	1.00000	−1.02846
0.00000	0.00000	0.00000	0.00000	0.00000	1.00000

[a] Starting from the objects slits (see fig. 2).
[b] Nominal tuning (no kinematics).

2.1.1. Tuning with kinematics

As discussed in section 1.4, when the reaction presents kinematic effects, the only first order adjustment is the position of the horizontal focus. It is moved in adjusting the first two quadrupole lenses (QA1 and QA2). Under these conditions, the vertical focus is kept on the target and the position of the intermediate horizontal focus moves in front of the dipole. In such a case, the first order resolution degrades, as shown in table 2. If necessary, it can be controlled via the setting of the horizontal object slit aperture. The second order effects can be adjusted by changing the dipole (DA) electrical shim currents.

2.2. The spectrometer (see figs. 1, 2 and 4)

Its nominal characteristics are given in table 3, together with the first order matrix elements for zero kinematics.

Table 2
Variation of the first order resolution of the incident beam line with different tunings, according to kinematics

$K = \frac{1}{p}\frac{dp}{d\theta}$	Momentum resolution [a] FWHM
0.0	3.4×10^{-5}
0.2	6.3×10^{-5}
0.3	8.0×10^{-5}
0.5	10^{-4}

[a] Values obtained for the nominal object size (FWHM = 2 mm).

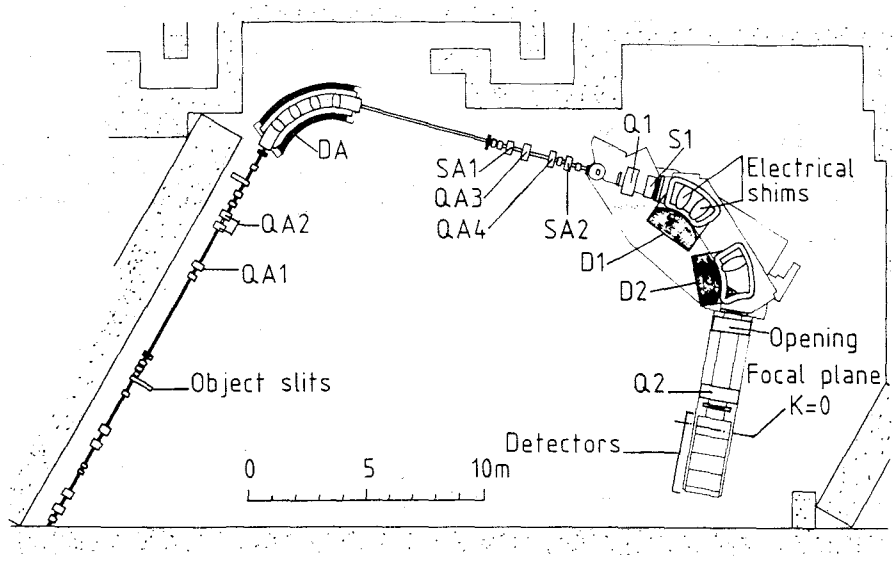

Fig. 2. Overall drawing.

The main elements are: an entrance quadrupole (Q1), two dipoles (D1 and D2) and an exit quadrupole (Q2).

The quadrupole Q1 is horizontally defocusing and controls the vertical optics inside the dipoles (see fig. 4). The vertical focusing is achieved via the second dipole exit face angle. The quadrupole Q2 controls the angular dispersion at the focal plane (cf. figs. 1–4). Second order corrections are obtained via: the entrance sextupole (S1), which is used to correct the (x/ϕ^2) aberration; the first dipole (D1) exit face curvature, which corrects the (x/θ^2) aberration once S1 has been adjusted; the second dipole (D2) exit face curvature, which controls the focal plane tilt angle. As the values of the (x/θ^2) and, near zero degree, (x/ϕ^2) aberration depend upon kinematic conditions, a second order adjustment can be done via two pairs of coils installed in dipole D1 ("electrical shims" in fig. 2) for S1 readjusted.

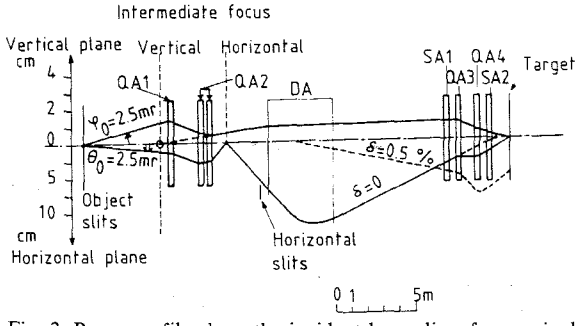

Fig. 3. Beam profile along the incident beam line, for nominal tuning (no kinematics). Beam emittance is assumed to be 5 π mm mrad in both planes, and object size to be 4×4 mm^2.

A third order correction is approximated in machining a different radius of curvature on each side of the optical axis, at the first dipole exit face (see table 3).

3. Description of the magnetic elements, shimming

3.1. Dipole DA

This is a window-frame-type magnet (see fig. 5).

Four pairs of mechanical shims (thickness 1.5 mm) have been installed inside the dipole, as shown schematically in fig. 6. They have been glued and screwed on the polar pieces. Their exact shapes have been adjusted according to field mapping measurements [4,5]. Remaining aberrations have been calculated, using the code ZGOUBI [6], to be at most 3×10^{-5} in momentum. This has been confirmed by experimental measurements (see section 6.1). Each mechanical shim is surrounded by a coil. In adequately setting the current in these four pairs of coils, one can simulate a variation of the mechanical shim thickness, providing adjustable second order corrections which are needed according to kinematic conditions. The whole set of coils is connected to a single power supply, in a serial arrangement. They are mounted outside the vacuum chamber.

The entrance and exit faces have antisaturation profiles. Vertical field clamps, magnetically connected to the dipole, were installed at each end, as shown in fig. 7a. Measurements have shown that the magnetic length did not vary with the induction level.

3.2. Dipoles D1 and D2

As already mentioned, the two dipoles have a C-shape (see fig. 8). Their main coils are serially connected to a

Table 3
(1) Nominal characteristics of the spectrometer

Nominal dispersion [a] (for Q2 nominal tuning)	[m]	8.1
Horizontal magnification		0.8
Vertical magnification		4.7
Horizontal acceptance	[mrad]	±35
Vertical acceptance	[mrad]	±35
Solid angle	[msr]	4.9
Mean bending radius	[m]	2.4
mean deflection angle	[deg]	2×42.5 = 85
D2 exit face angle	[deg]	24
D1 exit face curvature radii	[m]	R1 = 1.31
	[m]	R2 = 1.44
D2 exit face curvature radius	[m]	−1.67
Pole gap of the dipoles	[mm]	180
Maximum induction in the dipoles	[T]	1.2
Power required for max. field	[kW]	300
Weight of each dipole	[t]	70
Analysed momentum range	[%]	7
Length of focal plane	[cm]	60
Tilt angle of focal plane (straight focal plane)	[deg]	8
Focal plane displacement with kinematics ($K = 1/p)(dp/d\theta$) for Q2 nominal tuning	[m]	(7×K)
Angular range	[deg]	−10 to +105

(2) Transport matrix elements of the spectrometer [b]

−0.80216	−0.00049	0.00000	0.00000	0.00000	8.10788
−5.18622	−1.24345	0.00000	0.00000	0.00000	−0.00000
0.00000	0.00000	−4.70720	0.00000	0.00000	0.00000
0.00000	0.00000	−5.81954	−0.21261	0.00000	0.00000
−4.20492	−1.00817	0.00000	0.00000	1.00000	−1.94554
0.00000	0.00000	0.00000	0.00000	0.00000	1.00000

[a] Variable via Q2 tuning.
[b] For no kinematics.

single power supply. Each dipole has a pair of additive coils, to allow, if wanted, independent adjustments of the induction levels. The exact shape of the entrance and exit faces of the polar pieces have been decided after analysis of field measurements performed on a 1/4 scale moment magnet [7]. They were machined with antisaturating profiles, such as shown in fig. 7b. Field clamps were also mounted in regard of each face (see figs. 7b, 9 and 10). The position and the shape of their horizontal parts, initially machined identical to the corresponding polar face, and installed at a distance of one

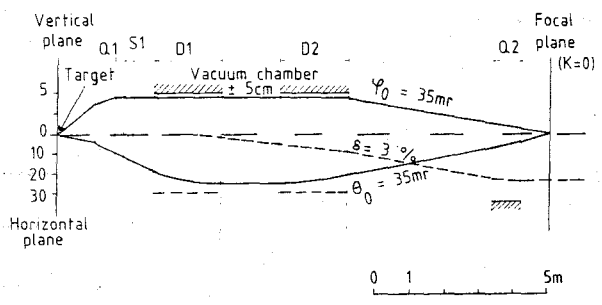

Fig. 4. Ion trajectories in the spectrometer.

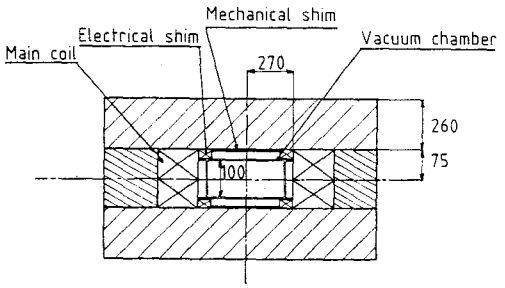

Fig. 5. Vertical cross section of the analysing magnet (DA). Distances are given in millimeters.

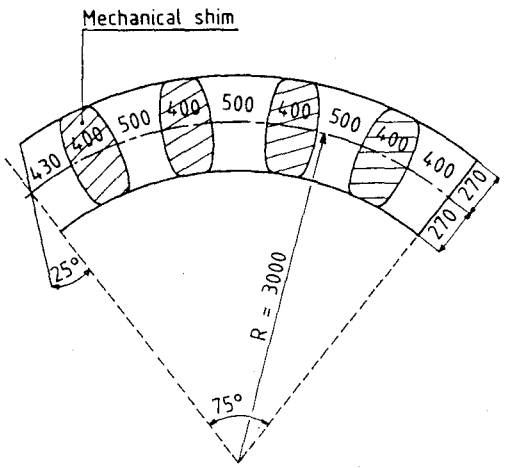

Fig. 6. Schematic horizontal cross section of the analysis magnet. Distances are given in millimeters.

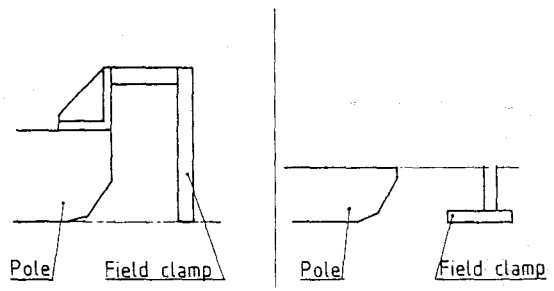

Fig. 7. Vertical cross section of the entrance (or exit) face of (a) the analysis magnet DA, (b) the dipoles D1 and D2 of the spectrometer.

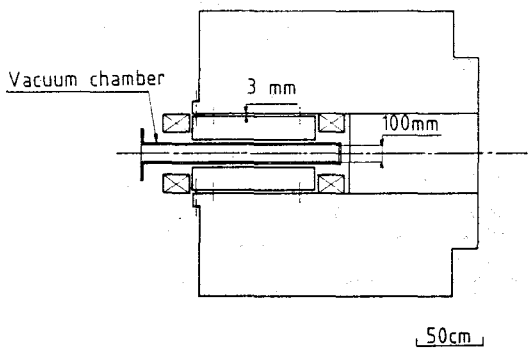

Fig. 8. Schematic cross section of a dipole (D1 or D2).

pole gap from the poles, have been used later on as variable parameters to adjust the field boundaries (see section 3.2.2).

As described below, mechanical shims were installed to correct for saturation effects at 1 T induction value, and additive coils were designed and installed to provide adjustable corrections needed for other induction levels [8].

3.2.1. Mechanical shims

The inner and outer sides of the polar surface have been machined such as shown in fig. 11 to avoid a too fast falling off of the induction. Field measurements in

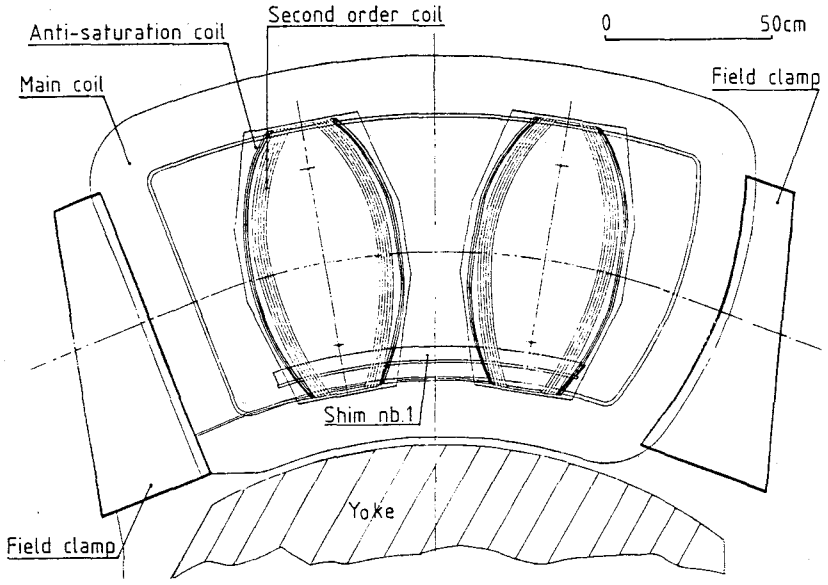

Fig. 9. Horizontal cross section of dipole D1.

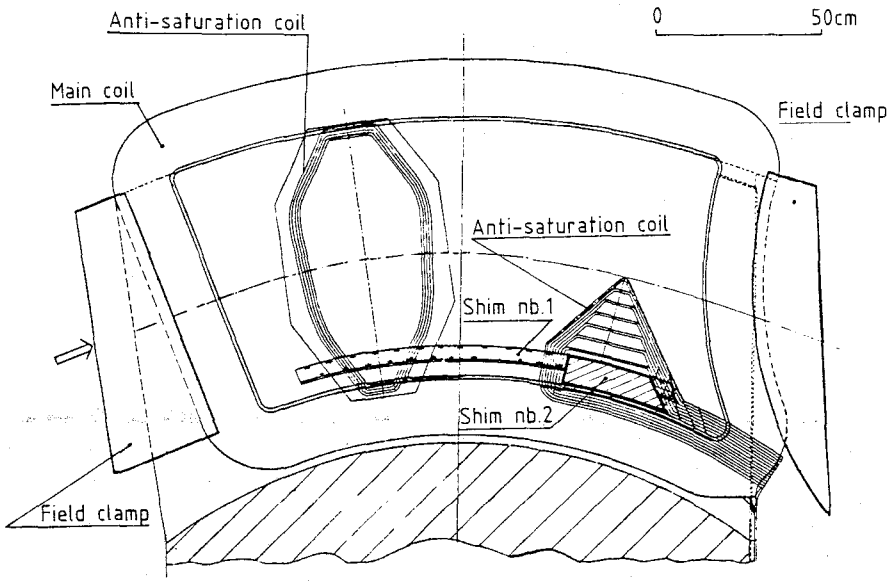

Fig. 10. Horizontal cross section of dipole D2.

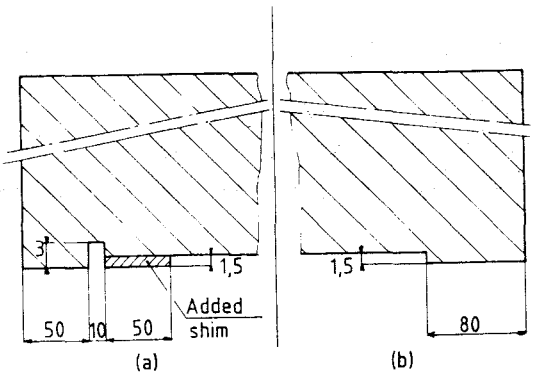

Fig. 11. Details of D1 and D2 inner (a) and outer (b) polar face cross sections. Distances are given in millimeters.

both dipoles indicated that additive corrections were needed along the inner radius.

In both dipoles, one mechanical shim – 1.5 mm thick, 50 mm wide – was glued and screwed all along the pole (shim labelled 1 in figs. 9 and 10). At the inner corner of the second dipole exit face, a stronger field gradient has to be compensated by a short thicker shim – 10 mm thick, 350 mm long, 110 mm wide (shim labelled 2 in fig. 10). These shims were calculated to provide the needed correction for an induction of 1 T.

3.2.2. Field clamp adjustments

The exact shapes of the horizontal parts of the field clamps have been deduced from field measurements in D1 and D2 at 1 T induction level, using an analytical method described in ref. [9]. Ray-tracing calculations using measured field maps have shown that this shimming procedure has improved the aberration values from 5×10^{-4} down to 5×10^{-5} (see fig. 12).

3.2.3. Saturation effects

At induction levels different from 1 T, ray-tracing calculation results obtained using real field maps revealed variable saturation effects. At 1.2 T, the aberration values increased up to 7×10^{-4} for D1 alone and to 4×10^{-3} for D2. Two independent corrections had to be obtained. First, in the sharp inner corner of D2 exit face, a pair of approximately triangular coils was designed, surrounding the already installed mechanical shims. Secondly, corrections were needed, identically in both dipoles, all along the inner and outer radii. They are obtained using additive coils with an adequate shape: one pair in D2 (4 turns in each coil), such as shown in fig. 10, and two pairs in D1 (2 turns in each coil), mounted in the already existing holders used for the second order electrical shims mentioned above (section 2.2). A single power supply is used, in order to get the same number of ampere-turns in the two dipoles. The amplitudes of the two described corrections (i.e. the current in the coils) are a nonlinear function of the induction level.

3.3. Quadrupole and sextupoles

The main characteristics of the various lenses are given in table 4, and cross sections of Q1, S1 and Q2 lenses are shown in fig. 13. See also refs. [10–12] for further details.

4. Practical tuning of the magnetic elements

All power supplies are computer controlled. Each one can be either set manually from the experimental room, or automatically adjusted via several computer tasks, as described below.

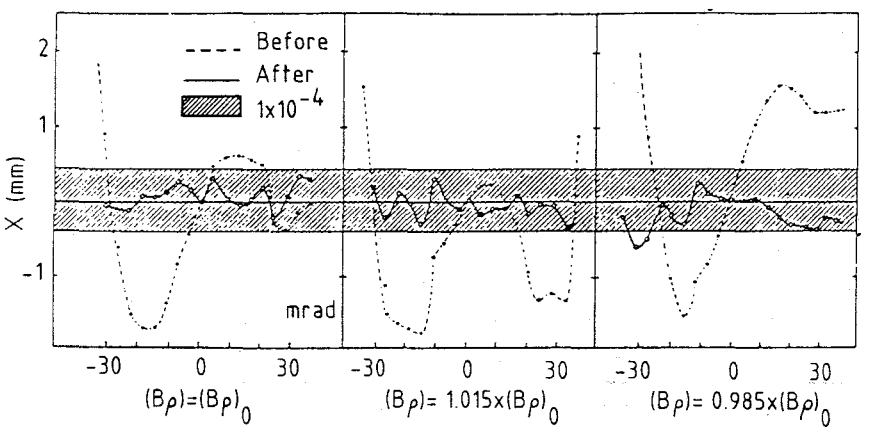

Fig. 12. Calculated position in the focal plane as a function of the initial direction θ, for 1 T induction value in the spectrometer, before and after adjustments of the field clamp shapes.

Table 4
Lens characteristics

Element	Pole aperture [mm]	Maximum induction [T/m]	Theoretical magnetic length [mm]	Remarks
Beam line				
Quadrupole QA1	100	8	300	
Quadrupole QA2 [b]	100	8	600	
Quadrupole QA3	140	6	300	
Quadrupole QA4	140	6	300	
Sextupole SA1	140	15 [a]	325	
Sextupole SA2	140	15 [a]	325	
Spectrometer				
Quadrupole Q1	240	5.5	610	C-shape [10]
Sextupole S1	360	4 [a]	410	C-shape [11]
Quadrupole Q2	800	1.44	740	Collins-type [12]

[a] In T/m^2 for sextupoles.
[b] Split into two lenses, identical to QA1.

4.1. Tuning of the dipoles

According to the value of the magnetic rigidity, the inductions in DA, D1 and D2 are reached using predetermined hysteresis cycles, which ensures the field map's reproducibility. Tuning of D1 and D2 concerns only their main coils, i.e. a single power supply.

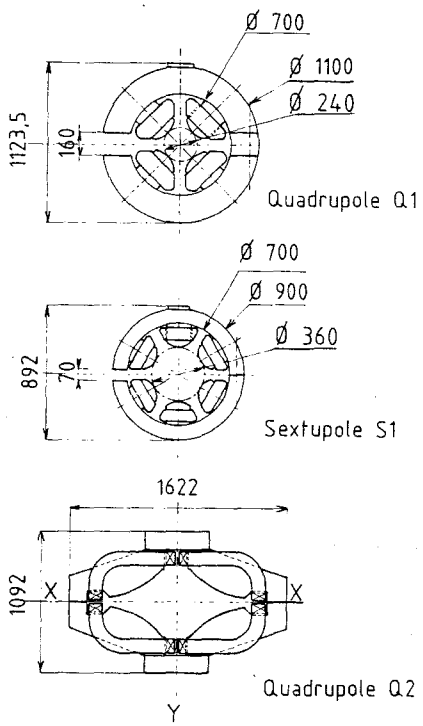

Fig. 13. Cross sections of Q1, S1 and Q2 lenses. Distances are given in millimeters.

4.2. Tuning of lenses and correction coils

According to the value of the magnetic rigidity of the incident ions, the tuning of the beam line lenses (including the shim coils in DA) are set to the proper values, corresponding either to no kinematic effect (i.e. horizontal focusing on target), or, if asked, to a given value of the first order kinematic coefficient K ($K = \mathrm{d}p/p \cdot \mathrm{d}\theta$), i.e. horizontal focus displaced by changing the current in QA1 and QA2.

Except for the power supply of the main coils (see section 4.1), all the other power supplies related to the spectrometer can be set simultaneously according to the value of the magnetic rigidity of the detected ions. This adjustment is done assuming no correction due to kinematics, since most experiments are performed at very small angles, or even at zero degree, where the second order corrections are no longer linear dependent upon the first order kinematic coefficient K. Up to now, there was no attempt to find an automatic procedure taking into account kinematic effects to set the current in the sextupole S1 and the second order coils installed in D1. Manual adjustments are done in looking at two-dimensional plots (x, θ) obtained easily from elastic scattering reactions with kinematic conditions close to those of the reaction under study, as illustrated in section 6.

4.3. Determination of the analysing beam line tuning

The tuning of QA3 and QA4, which controls the dispersion matching with the spectrometer, has been checked once for all (section 4.1).

The horizontal focus position can be checked easily for any kinematic condition, as follows:

A horizontally steering dipole has been installed close to the object slits. The first order matrix coefficient (x/θ) between this location and the horizontal focus is never larger than 0.009, whatever the kinematic conditions. In other words, the steerer does not act significantly on the position x of the focus, but only on the beam direction. So, when the beam line is correctly tuned for a given kinematic coefficient, the position, in the spectrometer focal plane, of the corresponding reaction peak is independent of the setting of the steerer (i.e. independent of the beam direction, which means that the beam divergence will not affect the resolution). A fast procedure was developed to check if this condition is satisfied or, if not, to readjust QA1 and QA2.

5. Main facilities (see also ref. [13])

5.1. Rotation of the spectrometer

The support of the spectrometer is equipped with air pads, which allow it to be lifted up and be rotated via a motorized driving wheel, from $-10°$ to $+105°$. It is made of two sections: the main section, on which are installed Q1, S1, D1, D2 and the corresponding vacuum chambers (shown in fig. 14) and a secondary section, on which are installed Q2 and the remaining vacuum chambers up to the detection area (see fig. 2). The two sections are linked together via an articulated horizontal axis, which allows them to have independent vertical displacements.

The medium plane is defined by three points: (1) the axis of rotation, which supports 40 t via a spherical articulation and (2) two articulated feet. Its exact position depends upon the angular setting, because of ground level variations. The medium plane of Q2 and detectors is automatically adjusted via a motorized hydraulic jack installed underneath the secondary section of the support.

The target holder is directly connected to the ground. Measurements have shown that the beam spot position on the target moves by less than 0.1 mm with respect to the spectrometer when rotating over the full angular range.

The body of the target chamber is bound to the spectrometer, and its connection to the beam line is realized via a sliding foil.

5.2. Experimental facilities

As indicated in figs. 2 and 14, many openings are provided. They allow easy access to any part of the ion trajectories and installation of various experimental setups such as detector, beam stops, collimators, screens, stripping foils, etc. Three large valves (100 mm high, 800 mm wide) have been designed to separate the vacuum chambers into four independently pumped areas: the target chamber, the D1 and D2 vacuum chamber, the Q2 area and the detector area.

5.2.1. The target area (see fig. 14)

This starts at the sliding foil and extends up to the entrance of the dipole vacuum chamber.

As seen in fig. 14, the shape of the vacuum chamber is quite complex. Room has been made as large as possible around the target, in order to accommodate bulky detector setups (parallel plates, ionization chambers), and to provide roughly a 1 m distance for time of flight measurements. Several motorized holders are available: two short arms (B1 and B2, 20 cm long) are connected to the ground, and are thus not moving with

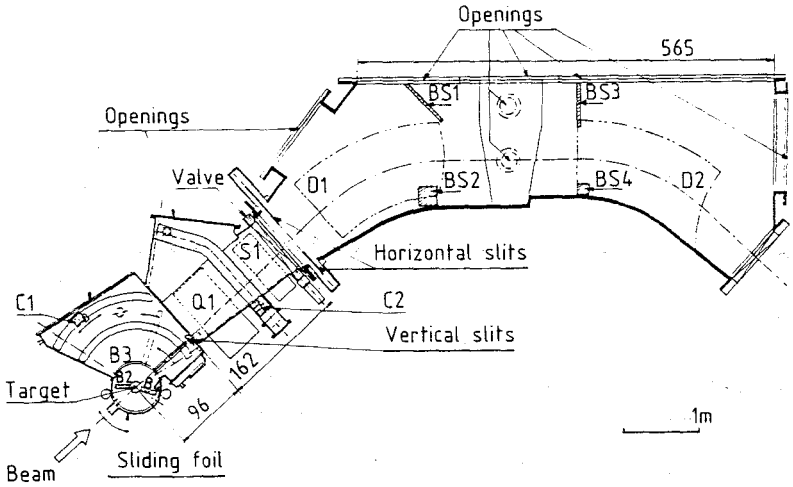

Fig. 14. Horizontal cross section of vacuum chambers of the spectrometer. BS stands for beam stop.

the spectrometer. A longer arm (B3) is supported by a circular rail fixed on the vacuum chamber, and, is thus moving with the spectrometer. Two lengths are possible: either 850 mm, movable from $-10°$ to $+105°$, or 1000 mm, movable from $+30°$ to $+105°$ (angles measured with respect to the optical axis of the spectrometer). There is also a carriage (C1) moving along a circular rail (radius 1200 mm) fixed on the vacuum chamber; and finally another carriage (C2), on which a well shielded Faraday cup is usually mounted, is installed between Q1 and S1.

The spectrometer acceptance is controlled by two pairs of adjustable slits: the vertical ones in front of Q1, the horizontal ones at the entrance of the first dipole. They are made of 1 cm thick stainless steel electrically insulated from the vacuum chamber. The horizontal slits are covered with 3 mm tantalum, thick enough to stop any incident beam. The maximum angular acceptance is $\pm 2°$ in both planes. But the horizontal slits can be opened up to 6° on the right hand side and 11° on the left hand side (looking downstream) in order to eventually stop the incident beam somewhere inside the dipole area, for spectrometer settings between $-6°$ and $+11°$.

5.2.2. Beam stops

For standard measurements, in most cases the beam is stopped in the Faraday cup mounted on C2 (fig. 14). This cup includes a shielding of about 10 cm of stainless steel. A beam profile monitor is mounted on its front, so as to check the beam position and to control instabilities. This beam stop allows the angular distributions to be measured down to 0.5.

Besides this, four beam stops are provided inside the dipole area, as shown in fig. 14 (BS1 to BS4). They are made of stainless steel covered with 3 mm thick tantalum, electrically insulated from the vacuum chamber. They are very useful for small angle and zero degree measurements (see section 6.2.4). In that case, the detectors in the focal plane and around the target are well shielded by the yokes of the dipoles against neutrons and gammas emitted from the beam stops. The horizontal slits can also be used as beam stops for measurements between $-6°$ and $+11°$.

5.3. Focal detector setting

Several kinds of detectors are used, either together or separately, according to the experiment. They have a useful area of 80 cm wide over 10 to 12 cm high. The vacuum chamber consists of four independent modules, each one around 70 cm long, and which can be assembled together as required.

5.3.1. Position measurements

These are usually done with detectors which include a drift chamber, for vertical position measurements, and a proportional counter equipped with a stripped cathode connected to a delay line for horizontal position measurements [14]. The accuracy is around 0.5 mm vertically, and less than 0.6 mm horizontally (see, for instance, section 6.2.1 and fig. 17). Two such detectors can be used, mostly set in front of and behind the focal plane.

5.3.2. Energy loss and energy signals

These can be obtained from an ionization chamber (70 cm deep) filled up with isobutane at a pressure of typically 500 mbar. It includes three position measurements and three energy loss signals (the anode is split into three parts, as described in ref. [15]). The resolution ranges from 1.3% to 1.6% for energy loss signals, and from 0.8% to 1.1% for energy signals, measured with stopped ions such as $27A$ MeV ^{40}Ar.

For ions that are not stopped, a 2 cm thick plastic detector behind the ionization chamber provides an energy resolution of 2% for oxygen and 3% for argon ions. In this case particle identification may be obtained using the ionization chamber for the dE signal and the plastic detector for the E signal. This identification is mainly used for the atomic number determination.

5.3.3. Time signals

For mass identification, a time of flight measurement is necessary.

In most experiments, the rf signal of the accelerator is used as start signal for time of flight measurements. The beam has a time structure of beam pulses about 100 ns apart and with a width of 0.2 to 1.5 ns. The time of flight being around 140 ns typically, this provides good enough resolution for most cases. Alternatively, one can use an avalanche counter installed at the exit of D2 (see the opening quoted in fig. 2), so as to avoid possible jitter effects between rf signals and beam pulses. Of course, one has to take into account charge exchange, energy and angular straggling effects in the first counter, and the reduction of the flight path (at most 5 m instead of about 14 m).

Different methods are currently used for getting a fast stop signal. It can be obtained by a parallel plate avalanche counter that provides, besides the time signal having an intrinsic resolution of about 350 ps, a position measurement with 1–2 mm resolution. For heavy particles such as Ar or Kr the cathode signal of the ionization chamber may be used for a fast timing with a resolution of 2–3 ns. In most cases, the easiest way to obtain the fast stop signal is provided by the plastic detector, which has an intrinsic resolution of about 350 ps.

5.3.4. Examples of identification functions

The time of flight in the spectrometer depends on the scattering angle with a coefficient of 1 cm/mrad.

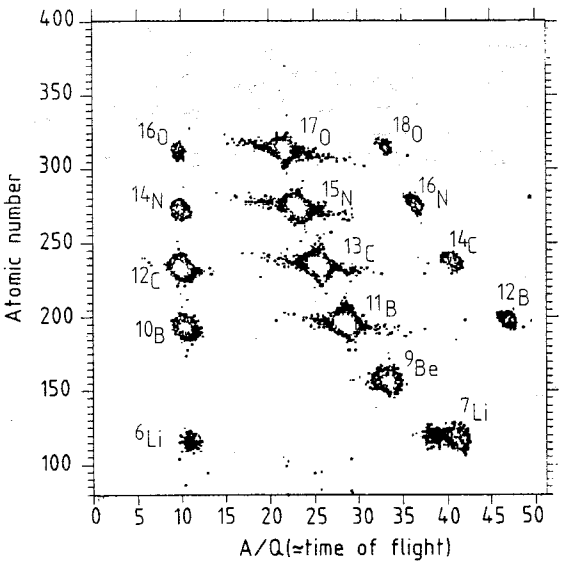

Fig. 15. Particle identification matrix plot: atomic number vs A/Q ratio (arbitrary units).

This corresponds to a variation of the time of flight of the order of 5% for the full solid angle. A software correction is done on-line to eliminate this effect. In the same way, atomic number identifications are improved using software. Standard programs were developed to do this, together with the calculation of the intersection of the particle trajectory with the focal plane.

A typical example of the particle identification scatter plots is shown in fig. 15.

6. Experimental measurements

6.1. Direct beam measurement

The spectrometer being set at zero degree, the incident beam has been transported up to the focal plane. A beam profile monitor has been mounted as a detector, on a movable carriage. The horizontal image size was smaller than the wire spacing. So, its shape has been deduced from intensity measurements on a single wire set at different positions. Three successive measurements were performed, on three consecutive wires, as shown in fig. 16. The mean value of the full width at half maximum is 3.2×10^{-5} in momentum. This is equal to the first order image size. So, the aberrations of the beam line are certainly smaller, in agreement with ray-tracing calculations (see section 3.1).

The aberrations of the spectrometer were not fully checked, because the phase space of the beam was too small compared to the acceptance (± 15 mrad horizontally and ± 2.5 mrad vertically to be compared to ± 35 mrad in both directions).

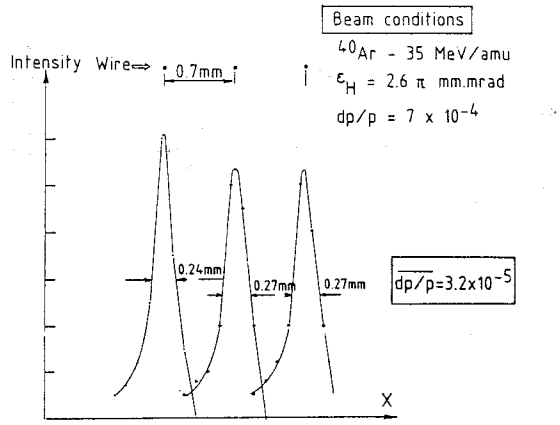

Fig. 16. Beam width measured in the focal plane of the spectrometer set at zero degree.

6.2. Examples of experimental results

6.2.1. Measurement with small kinematic effects

Using a 44A MeV ^{40}Ar beam on a ^{197}Au target, at full solid angle, the elastic scattering has been measured. The spectrometer was set at 4°. Two-dimensional plots of x versus θ and x versus ϕ did not reveal any visible aberration. The projected spectrum shown in fig. 17 shows a momentum resolution of 8×10^{-5}, better than the initial requirement (10^{-4}, see section 1.1).

6.2.2. Measurement with strong kinematic effects

An example is given in fig. 18. It shows a two-dimensional (x, θ) plot for elastic and inelastic scattering reactions induced by a 95A MeV ^{16}O beam on a target containing ^{12}C, ^{16}O, ^{28}Si and heavy impurity. Using two position signals provided by two detectors, the x values were calculated at the focal plane position corresponding to elastic scattering on ^{28}Si [16].

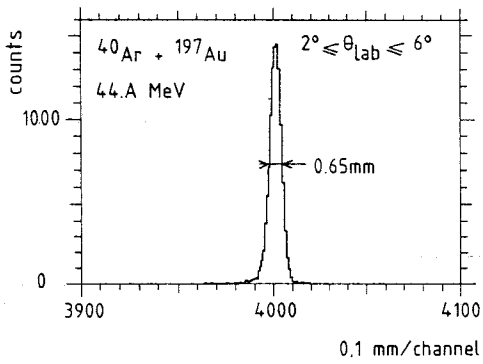

Fig. 17. Projected spectrum of elastic scattering measurement with negligible kinematic effect.

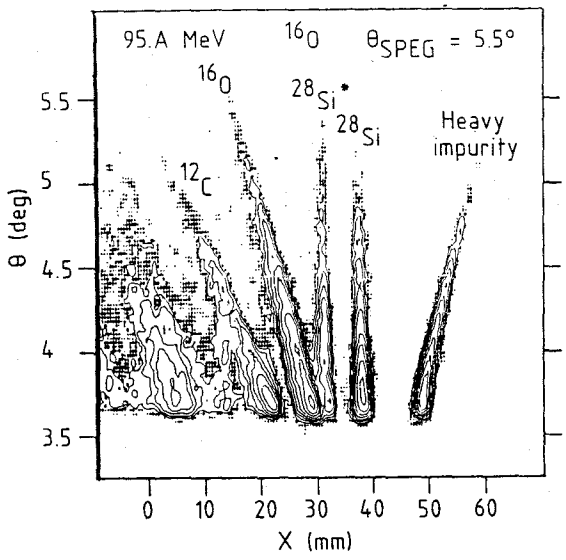

Fig. 18. Two-dimensional plot of elastic and inelastic scattering measurement, showing different kinematic effects.

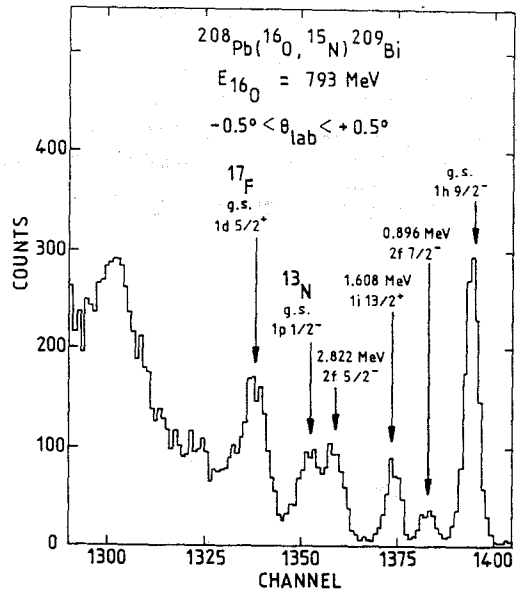

Fig. 20. Zero degree spectrum measured for the ^{208}Pb(^{16}O, ^{15}N)^{209}Bi reaction.

6.2.3. Angular resolution

Fig. 19 shows the angular distribution obtained for elastic scattering of ^{16}O on ^{28}Si. The angular resolution is seen to be at most 0.05°. The spectrometer was set at 3.5°, and the experimental points were obtained in a single exposure, using the full horizontal acceptance (±2°). The beam was stopped on the left hand side (downstream) horizontal slit. In order to get such an angular resolution, the incident beam has to be collimated so as to ensure a beam divergence not larger than 0.05° at the target. This was obtained in closing a pair of horizontal slits in front of the analysing magnet (DA). The angular calibration was previously measured, using a wire target together with a grid installed in front of Q1, so as to geometrically define a set of known angles.

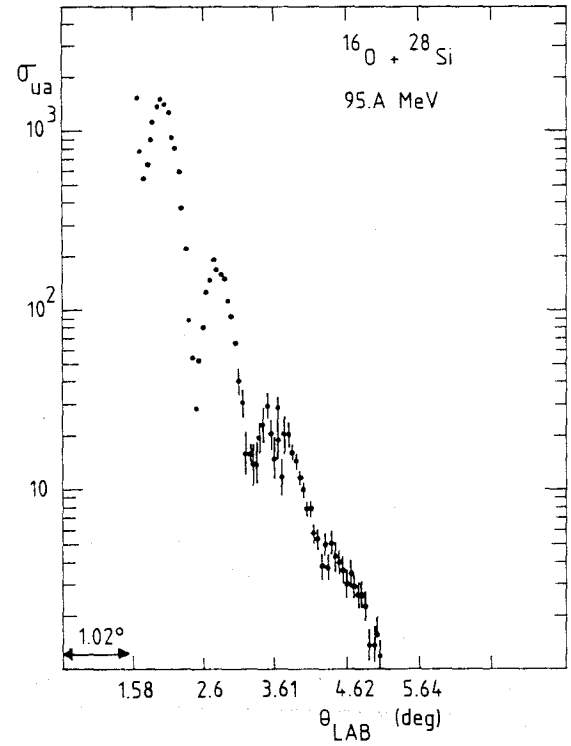

Fig. 19. Angular distribution obtained in a single exposure for elastic scattering of ^{16}O on ^{28}Si.

6.2.4. Zero degree measurement

An example is given in fig. 20, for a one-proton transfer reaction induced by a ~ 50A MeV ^{16}O beam on a ^{208}Pb target. Projectiles had a lower magnetic rigidity than ejectiles, so the beam could be stopped at the exit of D1 (on BS2, see fig. 14). The momentum resolution measured on the ground state peak is about 2×10^{-4} (FWHM), i.e. about 330 keV, mainly due to target effects.

7. Conclusion

The high resolution spectrometer SPEG was constructed for the National Heavy Ion Facility GANIL. The design goal (resolution of 1×10^{-4}) was obtained and surpassed. The use of the spectrometer and its detection system is user friendly. It proved to be a versatile instrument for nuclear reaction studies, mainly

leading to discrete nuclear levels. Example can be found in the Proceedings of the 3rd International Conference on Nucleus–Nucleus Collisions (Saint-Malo, France, June 1988). They contain nine contributions of work done with SPEG (contributions A-021, 31, 33, 35, 36, 39, 40, 41, 51), together with numerous references to other recent publications. Zero degree operation has become quite standard. An angular resolution better than 0.1° has been observed, which is necessary in the energy domain of GANIL. The excellent beam quality of the accelerator was essential for the good experimental conditions observed.

Acknowledgement

A magnetic spectrometer is an important project, which could not be realized without the participation of many persons. The authors want to thank all those who contributed directly or indirectly to this work.

References

[1] P. Birien and S. Valero, Note CEA-N-2215 (May 1981).
[2] J. Gastebois, Proc. Daresbury Study Week, ed.N.E. Sanderson, Daresbury Laboratory, DL/NUC/R19 (1979) p. 1.
[3] D.L. Hendrie, in: Nuclear Spectroscopy and Reactions, part A, ed. J. Cerny (1974).
[4] P. Bertrand et al., IEEE Trans. on Magn. 24 (1988) 946.
[5] W. Mittig and B. Fernandez, Compte rendu d'Activité du DPh-N (1983–1984) Note CEA N-2437 (1985) p. 276.
[6] D. Garetta and J.C. Faivre, DPh-N/ME, CEN-Saclay, unpublished.
[7] W. Mittig, Compte rendu d'Activité du DPh-N (1980–1981) Note CEA N-2276 (1982) p. 239.
[8] Compte rendu d'Activité du DPh-N (1984–1985) Note CEA N-2470, p. 251.
[9] B. Fernandez, A. Gillibert and W. Mittig, Rapport Ganil P. 85-05 (1985).
[10] A. Dael, CEN Saclay, Rapport Interne DPh-N/BE 80-312 (1980).
[11] A. Dael, CEN Saclay, Rapport Interne DPh-N/BE 80-254 (1980).
[12] R. Rebmeister, L. Arnold, G. Gaudiot, G. Swartz and A. Strasser, CRN Strassbourg, Rapport Interne CRN/PN 85-19 (1985).
[13] Compte rendu d'Activité du DPh-N (1984–1985) Note CEA N-2470, (1986) p. 245.
[14] B. Berthier and A. Le Merdy, Compte rendu d'Activité du DPh-N (1980–1981) Note CEA N-2276, 1982) p. 237.
[15] D. Disdier et al., CRN Strasbourg, Rapport d'Activité (1985) p. 112.
[16] P. Roussel, Thèse à l'Université de Paris-Sud (1986).